Atmos. Chem. Phys. Discuss., 4, 4339–4381, 2004
www.atmos-chem-phys.org/acpd/4/4339/
SRef-ID: 1680-7375/acpd/2004-4-4339

Atmospheric Chemistry and Physics Discussions

Investigation of inertia-gravity waves in the upper troposphere/lower stratosphere over northern Germany observed with collocated VHF/UHF radars

A. Serafimovich[1], **P. Hoffmann**[1], **D. Peters**[1], **and V. Lehmann**[2]

[1]Institute of Atmospheric Physics, Kühlungsborn, Germany
[2]Meteorological Observatory, Lindenberg, Germany

Received: 6 July 2004 – Accepted: 20 July 2004 – Published: 5 August 2004

Correspondence to: A. Serafimovich (serafimovich@iap-kborn.de)

Abstract

A case study to investigate the properties of inertia-gravity waves in the upper troposphere/lower stratosphere has been carried out over Northern Germany during the occurrence of an upper tropospheric jet in connection with a poleward Rossby wave breaking event from 17–19 December 1999. The investigations are based on continuous radar measurements with the OSWIN VHF radar at Kühlungsborn (54.1° N, 11.8° E) and the 482 MHz UHF wind profiler at Lindenberg (52.2° N, 14.1° E). Both radars are separated by about 265 km. Based on wavelet transformations of both data sets, the dominant vertical wavelengths of about 2–4 km for fixed times as well as the dominant observed periods of about 11 h for the altitude range between 5 and 8 km are comparable. Gravity wave parameter have been estimated at both locations separately and by a complex cross-spectral analysis of the data of both radars. The results show the appearance of dominating inertia-gravity waves with characteristic horizontal wavelengths between 600 and 300 km moving in the opposite direction than the mean background wind and a secondary less pronounced wave with a horizontal wavelength in the order of about 200 km moving with the wind. Temporal and spatial differences of the observed waves are discussed.

1. Introduction

The upper troposphere and lower stratosphere are characterized by the appearance of gravity waves with different scales. It is widely accepted that jet streams in the tropopause region itself are one of the main sources for these waves. Due to the exponential decrease of the density with the altitude, the upward propagation of the gravity waves is associated with an increase of their amplitudes till they are breaking. Associated with the wave breaking and the accompanying deposition of momentum and energy in the background flow, the dynamical and thermal structures above the source region up to the mesospheric heights as well as downward at tropospheric

ACPD

4, 4339–4381, 2004

heights are essentially influenced. However, the quantitative aspects of the propagation of the waves, their interactions with the mean winds and other waves as well as their generation are poorly understood at present. For a review on the current knowledge on gravity waves we refer to Fritts and Alexander (2003).

Particularly in the lower stratosphere, transport and mixing processes due to inertia-gravity waves (IGW) with frequencies close to the Coriolis frequency f are expected to be important, as shown by Plougonven et al. (2003). Here we are focusing on the investigation of these waves which can be characterized by periods of several hours and horizontal wavelengths of more than hundred kilometers. As reported by Sato et al. (1997), Thomas et al. (1999), Röttger (2000), inertia-gravity waves are observed in various regions of the Earth, they are connected with a number of different forcing mechanisms, such as ageostrophic adjustment, orographic forcing, frontal activity, deep convection or jet instability (Pavelin and Whiteway, 2002). These waves can alter the mean stratospheric temperature locally with amplitudes up to 10 K, which supports for instance at polar latitudes the generation of Polar Stratospheric Clouds during the winter months as investigated by Dörnbrack et al. (2002) and Buss et al. (2003).

A first case study to investigate the appearance of long period inertia-gravity waves in connection with a jet stream in the upper troposphere during a Rossby wave breaking event has been carried out at Kühlungsborn from 17–19 December 1999 in the frame of the LEWIZ campaign (Peters et al., 2003). The results were based on a series of 17 radiosondes released every 3 h supported by VHF radar observations at the same location. It has been found that the source of the dominating inertia-gravity wave with a period of about 12 h is placed in the region of the zonal wind jet just below the tropopause. To get more insight in the structure of gravity waves with shorter periods in the upper troposphere which cannot be resolved by 3-hourly radiosondes, the main objectives of this continuative study are directed to detailed analyses of the data of two VHF/UHF radars over Northern Germany at Kühlungsborn and Lindenberg, separated by about 265 km, and to examine the characteristics of inertia-gravity waves. Here we will consider both radars as 'collocated' due to the properties of the investigated inertia-

ACPD
4, 4339–4381, 2004

gravity waves, as their long horizontal wavelengths. To derive gravity wave parameters, different methods as wavelet transforms, hodograph analyses, rotary spectra and the Stokes-parameter technique have been tested and applied on the wind data at each radar location, available with a resolution of 30 min. These results are then compared with cross-spectral analyses of the data of both radars to identify common wave events and to discuss temporal and spatial differences of the observed waves in connection with the findings of Peters et al. (2003).

The paper is organized as follows. In Sect. 2 the meteorological background for inertia-gravity waves events is discussed and the parameters of the used radar are shortly described. Then we will summarize in Sect. 3 the used technique for data processing and the methods to estimate gravity wave parameters applied on the radar measurements at each location supplemented by the cross-spectral analyses of collocated radar measurements. Section 4 is devoted to the final estimation of inertia-gravity wave characteristics and the discussion of the results. In Sect. 5, we summarize our main results and give some concluding remarks.

2. Observations during a case study over Northern Germany from 17–19 December 1999

The investigations are based on observations made with two collocated radars, the OSWIN-53.5 MHz-VHF radar located at Kühlungsborn, and the 482 MHz-Wind profiler at Lindenberg. Details of the used radar parameter are summarized in Table 1.

The OSWIN VHF radar has been operating at Kühlungsborn since autumn 1999. The radar system was designed for continuous measurements and is running either in the spaced antenna (SA) or in the Doppler Beam Swinging mode (DBS). The antenna array consists of 144 four-element Yagis resulting in a transmitting half-power beam width of 6°. The beam is steerable in the vertical direction and towards the North, East, South, and West with a used off-zenith angle of 7°. For the investigations presented here, we used 1024 point complex time series sampled with 0.05 s. The radar

ACPD
4, 4339–4381, 2004

resolves a height region from 1 to 18 km. Data are averaged over 30 min for further investigations.

The 482 MHz Wind profiler belongs to the Meteorological Observatory Lindenberg of the German Weather Service (DWD). The Wind profiler is a fully coherent Doppler radar system with an additional RASS component to estimate sound virtual temperatures (Gurvich et al., 1987). It is in operation since August 1996 as a prototype system for a planned operational DWD profiler network (Lehmann et al., 2003). Wind measurements are carried out in the DBS mode using the vertical and four oblique beam directions with an off-zenith angle of 15°(Hogg et al., 1983). In contrast to the data processing technique used with the OSWIN VHF radar a statistical method for the incoherent integration of 17 individual spectra has been applied to reduce the noise variance and to suppress intermittent clutter contamination (Merritt, 1995).

The results have been obtained during a field campaign carried out from 17 to 19 December 1999. The meteorological situation was connected with a poleward Rossby wave breaking event and has been described in detail by Peters et al. (2003). The planning of the measuring campaign was based on the forecasts from the German Weather Service (DWD). During this period a strong eastward directed jet occurs over Northern Germany at 18 December 1999 in the upper troposphere as indicated in Fig. 1 by the temporal development of the zonal winds derived from the ECMWF data at 12:00 UT of the 17 and 18 December 1999 for the 300 hPa level corresponding to a height of approx. 9 km.

In Fig. 2 height time cross sections of the smoothed zonal and meridional wind are presented for both locations. The zonal wind over Kühlungsborn (Fig. 2a) increases until the 19 December, 00:00 UT and then decreases. The maximum jet stream reaches values of more than 50 m/s at heights between 6 and 10 km. The meridional component (Fig. 2b) shows a northerly wind with maximum values of more than 20 m/s at 18 December (12-18 UT) in coherence with the strong zonal jet but decays just before the zonal jet maximum occurs. The observations with the wind profiler at Lindenberg (Fig. 2c, Fig. 2d) separated by about 265 km from the Kühlungsborn VHF radar, show

ACPD
4, 4339–4381, 2004

the occurrence of the eastward and southward directed jets at nearly the same times and altitudes, whereas e.g. the reversal of the meridional winds to northward directed winds seems to be slightly stronger at Lindenberg. Detailed comparisons with the radiosondes (Peters et al., 2003) and the 6 hourly – ECMWF analyses winds (not shown here) result in good qualitatively agreements but the radar measurements resolves a higher variability due to the better time resolution. In the next section we will describe the data analysis techniques to derive wind perturbations necessary for the estimation of the gravity wave parameters.

3. Inertia gravity wave parameters estimation

3.1. Data processing to separate wind perturbations

The calculation of gravity wave parameters is based on wind perturbations, which have been estimated from the wind measurements after linear interpolations to substitute missing values. In general the perturbations can be described by variations of amplitudes a(x,z,t) of the wind components

$$a(x,z,t) = |a| \cdot \exp(i(kx + mz - \omega_{ob}t)), \quad (1)$$

where k and m are the horizontal and vertical wave numbers, respectively, and ω_{ob} is the wave frequency, observed at a fixed location. With the Doppler relation

$$\omega_{ob} = \omega_{in} + \overline{U}k, \quad (2)$$

ω_{ob} depends from the intrinsic frequency ω_{in}, the horizontal wave number k and the mean background horizontal wind component $\overline{U}$ given in the same direction as the horizontal wave number k. Corresponding to Zink and Vincent (2001), we adopt here the convention of a positive intrinsic frequency ω_{in} and define a negative vertical wave number m for waves propagating energy upwards.

ACPD
4, 4339–4381, 2004

Normally, the perturbations are characterized by a superposition of atmospheric waves with different frequencies. In order to estimate inertia-gravity wave parameters individual waves have to be separated or isolated by the application of reasonable band-pass filtering methods. To detect the presence of a wave in the data and to avoid arbitrarily choices of inappropriate filter parameters a wavelet transform has been applied (Torrence and Compo, 1998; Zink and Vincent, 2001). This technique is becoming a common tool for analyzing localized variations due to their possibilities to resolve the waves in frequency domain as well as in the time or height.

The term wavelets refers to a family of small waves generated from a single function, the so-called mother wavelet, by a series of dilations and translations. To be called a "wavelet" a function should be admissible. This means for an integrable function that its average should be zero. Wavelets are well localized in time and frequency spaces.

The wavelet transform itself denotes the correlation between the original function $f(t)$ and the version of the mother wavelet $g(\frac{t-b}{s})$, which is scaled with a factor s and translated by a dilation b. The choice of the mother wavelet is an important point in the wavelet transform. Since the horizontal wind perturbations of the gravity waves can be considered as amplitude-modulated sine waves, the selection of the Morlet wavelet seems to be reasonable, because the Morlet wavelet is nothing else than the plane wave modulated by a Gaussian. Its representations in time, $g(t)$, and Fourier space, $G(\omega)$, are given by

$$g_{\text{morlet}}(t) = \pi^{-1/4} e^{i\omega_0 t} e^{-t^2/2} \tag{3}$$

$$G_{\text{morlet}}(s\omega) = \pi^{-1/4} H(\omega) e^{-(s\omega-\omega_0)^2/2}, \tag{4}$$

where ω_0 is the nondimensional frequency, usually taken to be 6 to satisfy the admissibility condition (Farge, 1992), $H(\omega)$ is Heaviside step function, which is equal to 1 if $\omega>0$ and $H(\omega)=0$ otherwise, and s is wavelet scale.

ACPD
4, 4339–4381, 2004

By the convolution theorem, the wavelet transform was carried out in the Fourier domain and has been calculated by the inverse Fourier transform of the product:

$$W(t, s) = F^{-1}\left(G^*(s\omega)F(\omega)\right), \tag{5}$$

where $F(\omega)$ is the Fourier transform of the signal.

Wavelet transforms have been applied on time series of the zonal and meridional winds for constant height ranges as well as on wind profiles versus height for fixed time intervals. The significance of the results depends on the used mother wavelet and the sample length, which is reduced at the boundaries of the time and height intervals, respectively. To minimize such border effects, we decided to apply the Paul wavelet with the order of 4 on the wind profiles due to their short record lengths:

$$g_{\text{paul}}(t) = \frac{2^m i^m m!}{\sqrt{\pi(2m)!}}(1 - it)^{-(m+1)} \tag{6}$$

$$G_{\text{paul}}(s\omega) = \frac{2^m}{\sqrt{m(2m-1)!}} H(\omega)(s\omega)^m e^{-s\omega}, \tag{7}$$

where m is the order of the Paul wavelet. This wavelet leads to a better height localization of the dominant vertical wavelengths and smaller influences of the border effects, as shown by Torrence and Compo (1998). For the wavelet transform of the time series for constant heights we applied the Morlet wavelet with the order of 6 resulting in a better frequency localization of the dominant observed periods.

Because the wavelet functions are mostly complex, the wavelet transform $W(t, s)$ is also complex, therefore one can define the wavelet power spectrum as $|W(t, s)|^2$. It should be remarked that the wavelet scale s is not directly corresponding to a Fourier period λ. The relationship between the Fourier period and the equivalent wavelet scale can analytically be derived by substituting a cosine wave of a known frequency into Eq. (5) and calculating at which scale s the wavelet power spectrum has a maximum. For the Morlet wavelet with $\omega_0 = 6$, this leads to a value of $\lambda = 1.03s$ and for the Paul

ACPD
4, 4339–4381, 2004

wavelet of the order 4 this leads to a value of $\lambda = 1.39s$ (Torrence and Compo, 1998). Using Eq. (5) one can calculate the continuous wavelet transform for different scales s at all time points simultaneously to estimate efficiently the dependence of dominant periods on the time.

The results of the wavelet analysis are presented by the sum of wavelet power spectra of the zonal and meridional wind components in Fig. 3 measured at Kühlungsborn (a, b) and Lindenberg (c, d). From the wavelet transform of the wind time series averaged in the height, shown in the upper panel (a and c) of Fig. 3, we detect suitable similarities at both locations with significant periods between 6 and 14 h including a dominant observed period of about 12 h and a less pronounced period of about 6 h at 17 December. Furthermore, we find significant vertical wavelengths in the order of 2–4 km near the tropopause region from the wavelet transforms of vertical wind profiles averaged in time (b and d), for Kühlungsborn as well as for Lindenberg.

Evaluating these information from the wavelet transform now suitable filter parameters can be defined for different time and height ranges to identify the waves with distinct periods. The band-pass filtering has been carried out using the Fast Fourier transform to extract the signals with the dominant frequencies. We divided our analysis in two parts in order to investigate both frequency bands with periods of about 12 h and about 6 h, respectively. For the study of the waves with dominating observed periods of about 12 h the filter was constructed (case a) with a bandwidth of 8–18 h in the time and 2–4.5 km in the height, whereas in case (b) a filter with a bandwidth of 2–8 h in the time and 2–4.5 km in the height has been applied to study waves with periods of about 6 h.

In the first case (a), the resulting perturbations of the zonal winds at Kühlungsborn and at Lindenberg are shown in Fig. 4. From Eq. (1), the dashed lines indicate possible lines of constant phases of the dominant wind perturbations

$$mz - \omega_{ob}t = \text{const.} \quad (8)$$

indicating preferred downward phase propagations. The vertical and temporal distances between the phase lines correspond to the vertical wavelength and the ob-

ACPD
4, 4339–4381, 2004

served main period, respectively. The results for both locations agree nicely with the main findings from the wavelet analysis as shown in Fig. 3 with dominant periods of ∼12 h in the troposphere and vertical wavelengths of ∼3.3 km.

In the secondary case (b) to investigate those waves with periods of about 6 h, the results after the filter application on the meridional winds measured at Kühlungsborn and Lindenberg are shown in Fig. 5 leading to dominating downward phase propagating perturbations with observed periods of about 6 h and vertical wavelengths of about 3 km. In contrast to Fig. 4 the amplitudes are weaker at both locations as expected after the wavelet analyses represented in Fig. 3.

Both filtered data sets have been used in the following analyses to estimate gravity waves parameters.

3.2. Rotary spectra, hodograph- and Stokes analyses

For extracting IGW parameters three methods have commonly been used. The first method is the rotary spectrum, which was first applied to atmospheric IGWs by Thompson (1978). The second one, the hodograph analysis, is a standard tool in meteorology, described by (Gill, 1982) in connection with a rotating fluid and applied first to IGWs by Cot and Barat (1986). In addition, Vincent and Fritts (1987) presented a Stokes-parameter method and Cho (1995) developed a cross-spectral technique, which is in principle a spectral analogue of the Stokes-parameter analysis (Eckermann, 1996). All methods listed above were applied to estimate IGW parameters for both radar measurements carried out at Kühlungsborn and Lindenberg during this case study and are discussed in the next subsections.

3.2.1. Rotary spectra

The rotary spectrum is the complex Fourier transform of the complex velocity vector $UV(z)$, which is given by

$$UV(z) = u'(z) + iv'(z). \quad (9)$$

ACPD
4, 4339–4381, 2004

Since the direction of the rotation of the horizontal wind perturbations with the height indicates the vertical direction of inertia-gravity wave propagation, the presence of an inertia-gravity wave and their dominant vertical energy propagation can be estimated with the rotary spectra method (Cho, 1995). The spectra $F(UV(z))$ of the wind perturbations filtered with a bandwidth of 8–18 h in time and 2-4.5 km in height are presented in Fig. 6. They show in their negative parts the weaker clockwise rotational power corresponding in the northern hemisphere to an upward energy propagation and in their positive parts the larger counterclockwise rotational power corresponding to a dominating downward directed energy propagation, respectively, which is in agreement with the results of Peters et al. (2003) and Figures 6 and 10 therein, that the main source of these waves is the placed in the region of the zonal wind jet just below the tropopause. The spectra maximum occur at vertical wavelengths of about 3.3 km.

In contrast to these results, the rotary spectra of the wind variations filtered with a bandwidth of 2–8 h in the time and 2–4.5 km in the heights (Fig. 7) show a dominating upward energy propagation. We will discuss these results in context with the estimated wave numbers at the end of Sect. 4.

3.2.2. Hodograph analysis

The idea of hodograph analysis is to trace the course of the deviation of the horizontal wind vector with respect to height. If enough points are taken to span one wavelength of an inertia-gravity wave, then an ellipse can be fitted. For inertia-gravity waves, linear theory without any wind shear effects predicts

$$v' = -i \cdot u' \cdot \frac{f}{\omega_{\text{in}}}, \tag{10}$$

where u' and v' are the zonal and meridional components of the horizontal perturbation wind profiles, f is the Coriolis parameter and ω_{in} is the intrinsic frequency.

By the application of the hodograph one can extract the following parameters: the vertical sense of inertia-gravity wave propagation from the rotational sense; the direc-

tion of the horizontal wave propagation that is parallel to the major axis of the ellipse and, following Eq. (10), the intrinsic frequency, ω_{in}, from the ratio of the major to the minor axis of the ellipse. We have to note, that the horizontal wave propagation is uncertain with 180° without additional temperature information.

The hodograph analysis applied on the wind perturbations of 17 December 1999 to investigate the gravity waves with the observed periods of about 12 h and therefore filtered with a bandwidth of 8–18 h in time and 2–4.5 km in height (Fig. 8), shows a downward energy propagation in the troposphere from the anticlockwise rotational sense at Kühlungsborn and Lindenberg. We derived vertical wavelengths of about 3 km and intrinsic periods in the order of ∼7 and ∼12 h from the ratios of the major to the minor axis of the fitted ellipses at both locations, respectively. The differences between the hodographs for Kühlungsborn and Lindenberg can be caused by the variability of the background winds.

Using the wind perturbations filtered with a bandwidth of 2–8 h in the time and 2–4.5 km in the heights to investigate the waves with observed periods of about 6 h, the hodographs presented in Fig. 9 show intrinsic frequencies with corresponding periods between 6 and 8 h and upward energy propagations at both locations in agreement with the rotary spectra in Fig. 7. To demonstrate the stability of the wave propagation over a larger height range we have added in the right part (b) of the hodograph in Fig. 9 the wind perturbations from 4.25–7.7 km and from 11.0–14.25 km, showing the same vertical sense corresponding to upward directed energy propagation with increasing amplitudes at larger heights.

However, the hodograph method represents an instantaneous status and the estimation of gravity wave parameter is only valid for monochromatic waves. Usually a hodograph gives variable results due to the superposition of different waves in the wind profiles. One possibility to determine parameters of IGWs for a given wave number band averaged in time and height will be shown in the next section.

ACPD
4, 4339–4381, 2004

3.2.3. Stokes-parameter spectra

To receive a more statistical description of the gravity wave field the Stokes-parameter spectra as introduced by Vincent and Fritts (1987) and Eckermann and Vincent (1989) can be applied. This method arises from the analogy between partially polarized gravity waves and partially polarized electromagnetic waves (Kraus, 1966). To decompose the generally polychromatic wave field, the Stokes parameters are calculated in the Fourier domain (Eckermann and Vincent, 1989). A Fourier transform of the given vertical profiles $u'(z)$ and $v'(z)$ over their full height ranges yields the following Fourier representations of the profiles:

$$U(m) = U_R(m) + iU_I(m) \tag{11}$$

$$V(m) = V_R(m) + iV_I(m), \tag{12}$$

where m is the vertical wave number. From here, Eckermann and Vincent (1989) derived the following power spectral densities for the four Stokes parameters, based on the definitions:

$$I = A\left[\overline{U_R^2(m)} + \overline{U_I^2(m)} + \overline{V_R^2(m)} + \overline{V_I^2(m)}\right] \tag{13}$$

$$D = A\left[\overline{U_R^2(m)} + \overline{U_I^2(m)} - \overline{V_R^2(m)} - \overline{V_I^2(m)}\right] \tag{14}$$

$$P = 2A\left[\overline{U_R(m)V_R(m)} + \overline{U_I(m)V_I(m)}\right] \tag{15}$$

$$Q = 2A\left[\overline{U_R(m)V_I(m)} - \overline{U_I(m)V_R(m)}\right]. \tag{16}$$

Overbars denote time averages and A is a constant. The parameter P is the "in-phase" covariance associated with linear polarization, and Q is the "in quadrature" covariance associated with circular wave polarization, while I clearly quantifies the total variance and D defines its axial anisotropy. Consequently, any Stokes parameter

ACPD
4, 4339–4381, 2004

$X = \{I, D, P, Q\}$ can now be evaluated over the full range of heights within any wave number band.

$$X_{m_1,m_2} = \int_{m_1}^{m_2} X(m)\, dm. \tag{17}$$

Then the phase difference δ, major axis orientation Θ, averaged ellipse axial ratio R and degree of polarization d are given by

$$\delta_{m_1,m_2} = \arctan\left(\frac{Q_{m_1,m_2}}{P_{m_1,m_2}}\right) \tag{18}$$

$$\Theta_{m_1,m_2} = \frac{1}{2}\arctan\left(\frac{P_{m_1,m_2}}{D_{m_1,m_2}}\right) \tag{19}$$

$$d_{m_1,m_2} = \frac{\sqrt{D^2_{m_1,m_2} + P^2_{m_1,m_2} + Q^2_{m_1,m_2}}}{I_{m_1,m_2}} \tag{20}$$

$$R_{m_1,m_2} = \tan(\xi), \tag{21}$$

where

$$\xi = \frac{1}{2}\arcsin\left(\frac{Q_{m_1,m_2}}{d_{m_1,m_2}.I_{m_1,m_2}}\right). \tag{22}$$

The Stokes parameters calculated for the data from 17 December 1999 are presented in Tables 2 and 3 for both filtered datasets to investigate the gravity waves with periods at about 12 h and 6 h, respectively. As already mentioned in Sect. 3.2.2, the horizontal wave propagation determined by the major axis orientation Θ is uncertain with 180°without additional temperature information. Comparing the mean results derived for intervals of 5 h, we obtained at both locations similar parameters as e.g. the wave propagation directions represented by Θ_{m_1,m_2}. Note that the averaging times have been selected on the base of the times of maxima of the total variances described by

ACPD
4, 4339–4381, 2004

the Stokes parameter I, which characterize the mean kinetic energy for the investigated interval and vertical wave number band.

In Sect. 4 the obtained values are used for the final estimation of gravity waves characteristics at each radar location. To identify common wave events over a distance of ∼265 km, we will at first apply a simple cross-spectral analysis of the data of both radars.

3.3. Cross-spectral analysis

The cross-spectral analysis applied on the measurements of both radars can be used to identify common wave events and to investigate the characteristics of their horizontal propagation (e.g. wavelength or phase velocity) using the phase differences in the wind fluctuations between radars, provided that the wavelength can be resolved by the distance between both stations. After the detection of the appearance of dominating waves in both data sets with wavelet transform as shown in Fig. 3 the cross spectrum (Eq. 23) can be calculated

$$S_{U_1U_2}(\nu) = \frac{< U_1(\nu)U_2^*(\nu) >}{< |U_1(\nu)|^2 >^{\frac{1}{2}} < |U_2(\nu)|^2 >^{\frac{1}{2}}}, \quad (23)$$

where U_1 and U_2 are Fourier transforms of zonal wind measured by radars, ν is a independent variable in the frequency domain. The magnitude of $S_{U_1U_2}$ is a coherence function, which varies from 0 to 1. This gives a measure of the correlation between signals from both stations in a given spectral bin. Note that the ensemble averaging denoted by the brackets means that the cross spectrum is smoothed, because if no smoothing is carried out, the coherence, regardless of the nature of the processes, is equal to one. The phase value $\Delta\varphi$ corresponds to the time delay τ between the appearance of the wave maxima at both locations, which is given by

$$\tau = T_{ob}\frac{\Delta\varphi}{360^\circ}. \quad (24)$$

ACPD
4, 4339–4381, 2004

Here particular attention must be directed to avoid changes of the phases due to the application of any filtering procedures.

Usually to investigate the spatial characteristics of a wave one need at least three points forming a triangle. Such a method to analyse gravity waves moving across an array of surface-based meteorological atmospheric pressure sensors has been described by Nappo (2002). We applied here the cross-spectral analysis only for a pair of the radars, however using an additional information of the wave propagation direction α in relation to the connecting line between Radar 1 and Radar 2. Following the ideas of Nappo (2002), we consider a wave perturbation of some variable, Ψ, observed at each station. If we imagine a wave with constant amplitude and horizontal wave vector $\boldsymbol{k}$ observed at both stations, then the crests or any other phase point of the wave observed at Radar 1 (x_1, y_1) at the time t and at Radar 2 (x_2, y_2) at the time $t+\tau$ (Fig. 10) correspond to

$$\Psi_1\,(k_x x_1 + l_y y_1 + m_z z_1 - \omega t) = \Psi_2\,(k_x x_2 + l_y y_2 + m_z z_2 - \omega(t+\tau)), \tag{25}$$

where k_x, l_y, and m_z are the wave numbers in the $x-$, $y-$, and $z-$ directions, respectively. It is assumed that the wave does not change its main characteristics propagating from radar to radar, therefore we can write

$$k_x\, x_1 + l_y y_1 + m_z z_1 - \omega t = k_x\, x_2 + l_y y_2 + m_z z_2 - \omega(t+\tau), \tag{26}$$

which reduces to

$$k_x(x_2 - x_1) + l_y(y_2 - y_1) = \omega\tau - m_z(z_2 - z_1). \tag{27}$$

Equation (27) can be written in vector form as

$$\boldsymbol{k}\cdot\boldsymbol{S} = |k||S|\cos\alpha = \omega\tau - m_z(z_2 - z_1), \tag{28}$$

ACPD
4, 4339–4381, 2004

where $\boldsymbol{S}$ is the distance vector between both radars and α is the angle between $\boldsymbol{S}$ and the horizontal wave propagation vector $\boldsymbol{k}$ determined by the propagation direction Θ. Substituting $\omega_{ob} = 2\pi/T_{ob}$, the horizontal and vertical wave numbers by $L = 2\pi/k$ and $L_z = 2\pi/m_z$ to Eq. (27) we can write

$$L = \frac{|S|\cos\alpha}{\tau/T_{ob} - (z_2 - z_1)/L_z}. \quad (29)$$

Finally, using the distance between both radars $|S|$ and the time delay τ between gravity wave events, the ground-based horizontal phase velocity υ_{ph}^{ob} of the wave propagation can be estimated by

$$\upsilon_{ph}^{ob} = \frac{|S|\cos\alpha}{\tau - (z_2 - z_1)T_{ob}/L_z} = \frac{\omega_{ob}}{k}. \quad (30)$$

The cross-correlation spectrum of the zonal winds measured at Kühlungsborn and Lindenberg, presented in the left part of Fig. 11, has been averaged over the altitude range between 5.25 and 7.75 km. The amplitude of the cross spectrum shows a dominating common wave with an observed period of about 11.4 h which is in a good agreement with the dominating period estimated by the wavelet transforms of the time series at both locations as shown in Fig. 3a, c. The significance of this wave is proved by the coherency spectrum shown in the right part of Fig. 11. Due to the slopes of the phase lines in Fig. 4 and the downward energy propagation with a vertical wavelength of about 3.3 km (Fig. 6), the observed period of 11.4 h is negative (Eq. 8). The phase difference (red line in Fig. 11) of about $\pm 40^\circ$ or $\mp 320^\circ$ between the maxima of this wave at both locations corresponds to an amount of a time delay τ of about 1.3 h or 10.1 h, respectively, whereas the sign depends from the sign of the observed frequency itself.

To check the reliability of this method, we have applied Eqs. (29) and (30) using the radar coordinates and the observed period $2\pi/\omega_{ob}$ of −11.4 h. With the detected time delay of −1.3 h and +10.1 h, we found consistent values for the horizontal wave numbers k and ground based horizontal phase velocities υ_{ph}^{ob} directly estimated from the

ACPD
4, 4339–4381, 2004

cross-spectral analysis. In Table 4 the results are shown derived with different assumed wave directions Θ or the corresponding angle α. Furthermore we have used different height shifts $z_2 - z_1$ supported by mean vertical phase velocities with an amount of about 0.06–0.10 m/s in order to study the variability of the derived wave parameter. We define here and in the following that a wavelength will be negative if the corresponding wave number k or m are negative.

We started at first with a time delay of 10.1 h (case A) with the assumption that the wave is moving in the same direction as the jet-maximum at about 9 km, which differs from the zonal direction (case B) by only 6°. In both examples, the estimated horizontal wavelengths of about −634 km (case A) or −557 km (case B) for a height shift of about 2 km are in same order with the horizontal wavelength in the zonal direction estimated by Peters et al. (2003). Further a time delay of −1.3 h was used. In case (C) we have used the major axis orientation of the wave direction Θ≈54° estimated by the Stokes-parameter analysis applied for the dominating waves with periods of about 12 h and filtered with bandwidths between 8 and 18 h (see Table 2). Note that in this case the directions of the wave propagation at both locations differ by only 8° so that there are no ambiguities to estimate α and to apply the cross-spectral analysis. Applying a realistic height shift of about −500 m, in case (C) we obtained a horizontal wavelength of about −300 km and an observed horizontal horizontal phase speed of 7.5 m/s. We will discuss these results in the next Sect. 4 together with the results separately estimated at each radar location.

4. Gravity wave characteristics and discussion

To estimate the gravity waves characteristics such as intrinsic frequency ω_{in} and horizontal wavenumber k, the phase and group velocities for each radar location sepa-

ACPD
4, 4339–4381, 2004

rately, the following three relations will be used. The polarization relation is given by

$$R = \left| \frac{f}{\omega_{\text{in}}} - \frac{k}{m\omega_{\text{in}}} \frac{\partial \overline{V}}{\partial z} \right|, \tag{31}$$

where R is the averaged axial ellipse ratio, f is the Coriolis parameter, and z is the altitude. In contrast to Eq. (10) here the vertical wind shear effect in the background wind, as introduced by Hines (1989), is included by the term $\frac{\partial \overline{V}}{\partial z}$, where $\overline{V}$ denotes the mean horizontal wind component perpendicular to the wave propagation. This is important if the wave vector is nearly perpendicular to the back stream direction. The dispersion relationship is given by

$$\omega_{\text{in}}^2 = f^2 + \frac{N^2 k^2}{m^2} - \frac{2fk}{m} \frac{\partial \overline{V}}{\partial z}, \tag{32}$$

where N is the angular Brunt-Väisälä frequency. Finally, the Doppler relation is given by Eq. (2).

For a given location, the Coriolis frequency f has been calculated by

$$f = 2 \cdot 7.292 \cdot 10^{-5} \sin \varphi, \tag{33}$$

where φ is geographical latitude. The Brunt-Väisälä frequency $N(h)$ can be estimated from radiosonde temperature soundings, but here we are using mean values of 0.013 s^{-1} for the troposphere and of 0.021 s^{-1} for the stratosphere, respectively.

The mean background horizontal wind component in the direction of the wave propagation $\overline{U}$ and the horizontal wind component perpendicular to the wave propagation $\overline{V}$ are estimated by

$$\begin{aligned} \overline{U} &= U_x \cos\Theta + V_y \sin\Theta \\ \overline{V} &= -U_x \sin\Theta + V_y \cos\Theta, \end{aligned} \tag{34}$$

ACPD
4, 4339–4381, 2004

where U_x and V_y are the observed zonal and meridional winds, and Θ is the direction of the wave propagation calculated with Stokes-parameter analysis. Finally the vertical wind shear term $\partial\overline{V}/\partial z$ has been estimated.

The intrinsic horizontal and vertical components of the phase velocity are

$$\left(\upsilon_{\mathrm{ph}}, \upsilon_{\mathrm{pz}}\right) = \left(\frac{\omega_{\mathrm{in}}}{k}, \frac{\omega_{\mathrm{in}}}{m}\right). \tag{35}$$

The intrinsic horizontal and vertical components of the group velocity are given by

$$c_{\mathrm{gh}} = \frac{\partial\omega_{\mathrm{in}}}{\partial k} = \frac{N^2 k}{\omega_{\mathrm{in}} m^2} - \frac{f}{\omega_{\mathrm{in}} m}\frac{\partial\overline{V}}{\partial z} \tag{36}$$

$$c_{\mathrm{gz}} = \frac{\partial\omega_{\mathrm{in}}}{\partial m} = -\frac{N^2 k^2}{\omega_{\mathrm{in}} m^3} + \frac{fk}{\omega_{\mathrm{in}} m^2}\frac{\partial\overline{V}}{\partial z}. \tag{37}$$

The ground-based horizontal group velocity relative to observer is then given by

$$c_{\mathrm{gh}}^{\mathrm{ob}} = \frac{\partial\omega_{\mathrm{ob}}}{\partial k} = c_{\mathrm{gh}} + \overline{U}. \tag{38}$$

The observed frequency ω_{ob} and the vertical wave number m can be derived e.g. by wavelet transforms or spectral analyses of the wind measurements.

We have used two ways to solve the Eqs. (31), (32) and (2). If the ellipse ratio R and ω_{ob} are given then the intrinsic frequency ω_{in}, the horizontal wavenumber k and the vertical wavenumber m can be estimated by solving the polarization relation Eq. (31), the dispersion relation Eq. (32) and the Doppler relation Eq. (2). In the second way, the ellipse ratio R and the vertical wavenumber m are given by the evaluation of the spectra with respect to height. Then the Eqs. (31) and (32) have to be solved to estimate the intrinsic frequency ω_{in} and the horizontal wavenumber k.

To investigate the gravity waves with observed periods of about 12 h, we follow the first way to solve the Eqs. (31), (32) and (2) using the Stokes parameter shown in

ACPD
4, 4339–4381, 2004

Table 2 and the mean winds $\overline{U}$, $\overline{V}$ estimated with Eq. (34) from the dominating jet stream at the height of about 9 km (see e.g. Fig. 2). To resolve the ambiguities in the polarization relation Eq. (31) and in the quadratic dispersion relation Eq. (32) and to determine the signs of the wave numbers we used here additional the slopes of the constant phase lines Eq. (8) in the wind perturbations (Fig. 4) in comparison with the downward energy propagation as estimated by the rotary spectra (Fig. 6).

The derived gravity wave characteristics are given in Table 5, resulting in consistent parameters at both locations like the horizontal wavelengths as well as the group and phase velocities. The dispersion relation leads here to vertical wavelengths between 3.3 and 3.6 km, which are in the order of the results of the wavelet analyses (see Fig. 3) or the rotary spectra (Fig. 6). Note, that the relation

$$\upsilon_{\mathrm{ph}} = \frac{\omega_{\mathrm{in}}}{k} = \frac{\omega_{\mathrm{ob}}}{k} - \overline{U} \tag{39}$$

between the intrinsic and the ground-based horizontal phase speed is only fulfilled if the intrinsic phase speed υ_{ph} and hence the horizontal wavenumber k are negative.

Then the intrinsic phase velocities υ_{ph_c} estimated from the cross-spectral analysis, ($\upsilon_{\mathrm{ph}}^{\mathrm{ob}}$=7.5 m/s, see Table 4 and case C therein) for the wave direction against the background wind $\overline{U}$ and using the mean winds at both locations (Table 5) parallel to the wave direction

$$\upsilon_{\mathrm{ph}_c} = \upsilon_{\mathrm{ph}}^{\mathrm{ob}} - \overline{U} \tag{40}$$

yields values of −9.5 m/s and −10.5 m/s, which agree very well with the results υ_{ph} separately estimated for Kühlungsborn (−10.1 m/s) and Lindenberg (−10.3 m/s, see Table 5), respectively.

Thus, the results estimated for each radar location and leading to negative wave numbers k and horizontal wavelengths of about 300 km confirm the results derived directly from the cross-spectral analysis, using the mean wave directions estimated from

ACPD
4, 4339–4381, 2004

the Stokes-parameter analysis and a realistic height shift of −500 m corresponding to a mean vertical phase velocity υ_{pz} of about 0.1 m/s for the time delay of −1.3 h.

We have to note for the case investigated here, that the estimations of the horizonal wavelengths depend primarily on changes in the component of the mean background wind parallel to the wave direction as used in the Doppler relation Eq. (2), whereas the influence of the vertical wind shears effects used in Eqs. (31) and (32) leads to changes in the intrinsic period of 1.6 h and in the horizontal wavelength of about 40 km.

For the waves with observed periods of about 6 h the sign of ω_{ob} must be positive due to the slopes of the phase lines in Fig. 5 and the upward energy propagation (Fig. 7) (see Eq. 8). In this case we found self-contained solutions applying the second way based on a given ellipse ratio R and the vertical wavenumber m, estimated by the evaluation of the spectra with respect to height and using the Stokes-parameter shown in Table 3. The solution of Eqs. (31) and (32) leads to the estimation of the intrinsic frequency ω_{in} and the horizontal wavenumber k for a height of about 6 km as shown in Table 6. Note that in this case the sign of the wavenumber k must be positive to fulfill Eq. (39). Therefore we conclude that these less pronounced waves with horizontal wavelengths in the order of about 200 km are moving with the wind. Due to their upward directed energy propagation (Fig. 7) we can only speculate that a possible source for these waves could be connected with frontal activity or deep convection in the boundary layer.

We can summarize, that we found two wave classes with different energy propagation directions during this case study at both radar sites. Both wave classes show downward phase propagations. Connected with a jet stream in the upper troposphere, the dominating wave with an observed period −11.4 h shows a downward energy propagation in the troposphere. The analysis also shows that the direction of the wave propagation is upstream, and the intrinsic period is ∼8 h. Horizontal wave numbers for this wave are negative and vertical wave numbers are positive at both locations with corresponding wavelengths between −281 and −313 km as well as between 3.3 and 3.5 km, respectively. Additionally to this wave class, we detected another one with

ACPD
4, 4339–4381, 2004

shorter horizontal wavelengths and a smaller observed period of 6.4 h, which has an upward directed energy propagation. The horizontal and vertical wavelengths of this wave are ∼200 km and −3.2 km, respectively. For both wave classes the phases tend to be nearly "flow-aligned". Nevertheless, there exist also "flow-perpendicular" waves, which we discussed in Sect. 3.3.

5. Conclusions

In the frame of a case study to investigate the properties of inertia-gravity waves over Northern Germany in connection with a jet stream in the upper troposphere during a Rossby wave breaking event (Peters et al., 2003) we used continuous radar measurements with the OSWIN VHF radar at Kühlungsborn and the UHF Wind Profiler at Lindenberg. Both sites are separated by about 265 km. Wavelet analysis have been described and applied to consider the height and time dependence of the wave packages, to identify comparable inertia-gravity wave events at the two locations. Based on the estimated vertical wavelengths of about 2–4 km near the tropopause region from the wavelet transforms of the vertical wind profiles averaged in time, and the detected dominant observed periods of about 11–12 h together with a less pronounced period of about 6 h derived from the wavelet transform of the wind time series, suitable filter parameters have been specified to determine the wind perturbations applying the Fourier technique as filtering routine. We found for both periods dominating downward phase propagating perturbations. The rotary spectra as well as the hodographs indicate a downward directed energy propagation for the dominating period of about 12 h which is in agreement with the results of Peters et al. (2003), whereas the detected waves with periods of about 6 h show an upward directed energy propagation.

The Stokes-parameter analysis as the most reliable method to estimate first gravity parameter and the solution of the equations based on the linear theory lead to the occurrence of dominating gravity waves with characteristic horizontal wavelength between 600 and 300 km moving against the background wind and confirms the re-

ACPD
4, 4339–4381, 2004

sults estimated by Peters et al. (2003) which have been derived by a comparison of the observed frequency from a VHF radar and the intrinsic frequency from the radiosondes launched at the same location. Further, the occurrence of a secondary less pronounced wave with a horizontal wavelength in the order of about 200 km moving with the wind has been found using the Stokes analysis and solving the dispersion and polarization relation.

The independent analyses of the radar measurements at both locations lead to consistent results. The cross-spectral analysis between the data of both radars have been used to prove the coherence of a common wave event over the distance of about 265 km taking into account its vertical propagation and to estimate directly the horizontal wavelengths of −600 km for waves moving against the jet stream as well as of about −300 km as well as the corresponding phase velocities, which are in a good agreement with the results estimated separately at each location. In contrast to the way to solve the Eqs. (31), (32) and (2) as described in Sect. 4, this very simple method uses only the geometry, the phase differences of coherent waves at both locations and the mean direction of the wave propagation vector which should not significantly differ at both radar stations.

To avoid this latter condition and to get more statistical reliability, the usage of the data of more radar stations, e.g. including the DWD-UHF Wind profiler at Ziegendorf (Lehmann et al., 2003), in operation since January 2004 and forming a triangle with Lindenberg and Kühlungsborn over Northern Germany, should improve the investigations of the spatial gravity wave characteristics in future. Further investigations will be directed to compare the obtained results with the output of the mesoscale MM5 model, applied for the description of the dynamics for the selected events, and organized for neighboring locations with a sufficient resolution in time and height.

Acknowledgements. The authors thank W. Singer, D. Keuer and M. Zecha for the management and the support to operate the VHF radar at Kühlungsborn. Helpful discussions with C. Zülicke and M. Rapp are highly appreciated. The investigations are part of the LEWIZ project, supported by the German Ministry of Education and Research (BMBF) under the framework

program AFO 2000.

References

Buss, S., Hertzog, A., Hostetter, C., Bui, T. P., Lüthi, D., and Wernli, H.: Analysis of a jet stream induced gravity wave associated with an observed ice cloud over Greenland, Atmos. Chem. Phys. Discuss., 3, 5875–5918, 2003. 4341

Cho, J.: Inertio-gravity wave parameter estimation from cross-spectral analysis, J. Geophys. Res., 100, 18 727–18 737, 1995. 4348, 4349

Cot, C. and Barat, J.: Wave-turbulence interaction in the stratosphere: A case study, J. Geophys. Res., 91, 2749–2756, 1986. 4348

Dörnbrack, A., Birner, T., Fix, A., Flentje, H., Meister, A., Schmid, H., Browell, E., and Mahoney, M.: Evidence for inertia gravity waves forming polar stratospheric clouds over Scandinavia, J. Geophys. Res., 107, D20, 8287, doi:10.1029/2001JD000452, 2002. 4341

Eckermann, S.: Hodographic analysis of gravity waves: Relationships among Stokes parameters, rotary spectra and cross-spectral methods, J. Geophys. Res., 101, 19 169–19 174, 1996. 4348

Eckermann, S. and Vincent, R.: Falling sphere observations gravity waves motions in the upper stratosphere over Australia, Pure Appl. Geophys., 130, 509–532, 1989. 4351

Farge, M.: Wavelet transforms and their applications to turbulence, Annu. Rev. Fluid Mech., 24, 395–457, 1992. 4345

Fritts, D. C. and Alexander, M. J.: Gravity wave dynamics and effects in the middle atmosphere, Rev. Geophys., 41, 1, 1003,doi:10.1029/2001RG000106, 2003. 4341

Gill, A. E.: Atmosphere-Ocean Dynamics, Academic Press, 1982. 4348

Gurvich, A., Kon, A., and Tatarskii, V.: Scattering of elecromagnetic waves on sound in connection with problems of atmospheric sounding (review), Radiophys. Quant. Electron., 30, 347–366, 1987. 4343

Hines, C. O.: Tropopausal mountain waves over Arecibo: A case study, J. Atmos. Sci., 46, 476–488, 1989. 4357

Hogg, D., Decker, M., Guiraud, F., Earnshaw, K., Merritt, D., Moran, K., Sweezy, W., Strauch, R., Westwater, E., and Little, C.: An automatic profiler of the temperature, wind and humidity in the troposphere, J. Clim. Appl. Meteorol., 22, 807–831, 1983. 4343

Kraus, J.: Radioastronomy, McGraw-Hill, New York, 1966. 4351
Lehmann, V., Dibbern, J., Görsdorf, U., Neuschaefer, J., and Steinhagen, H.: The new operational UHF Wind Profiler Radars of the Deutscher Wetterdienst, in Proceedings of the Sixth International Symposium on Tropospheric Profiling: Needs and Technologies, Leipzig, Germany, edited by U. Wandinger, R. Engelmann, and K. Schmieder, pp. 489–491, Institute for Tropospheric Research, 2003. 4343, 4362
Merritt, D. A.: A statistical averaging method for wind profiler doppler spectra, J. Atmos. Ocean. Techn., 12, 985–995, 1995. 4343
Nappo, C. J.: An introduction to atmospheric gravity waves, Academic Press, 2002. 4354
Pavelin, E. and Whiteway, J.: Gravity wave interactions around the jet stream, Geophys. Res. Lett., 29, 21, 2024, doi:10.1029/2002GL015783, 2002. 4341
Peters, D., Hoffmann, P., and Alpers, M.: On the appearance of inertia gravity waves on the north-easterly side of an anticyclone, Meteor. Z., 12, 25–35, 2003. 4341, 4342, 4343, 4344, 4349, 4356, 4361, 4362
Plougonven, R., Teitelbaum, H., and Zeitlin, V.: Inertia gravity wave generation by the tropospheric midlatitude jet as given by the Fronts and Atlantic Storm-Track Experiment, J. Geophys. Res., 108, D21, 4686, doi:10.1029/2003JD003535, 2003. 4341
Röttger, J.: ST radar observations of atmospheric waves over mountainous areas: a review, Ann. Geophysicae, 18, 750–765, 2000. 4341
Sato, K., O'Sullivan, D. J., and Dunkerton, T. J.: Low-frequency inertia-gravity waves in the stratosphere revealed by three week continuous observation with the MU radar, Geophys. Res. Lett., 24, 1739–1742, 1997. 4341
Thomas, L., Worthington, R., and McDonald, A. J.: Inertia-gravity waves in the troposphere and lower stratosphere, Ann. Geophysicae, 17, 115–121, 1999. 4341
Thompson, R. O. R. Y.: Observation of inertial waves in the stratosphere, Quart. J. R. Met. Soc., 104, 691–698, 1978. 4348
Torrence, C. and Compo, G. P.: A practical guide to wavelet analysis, Bull. Amer. Meteor. Soc., 79, 61–78, 1998. 4345, 4346, 4347
Vincent, R. and Fritts, D.: A climatology of gravity wave motions in the mesopause region at Adelaide, Australia, J. Atmos. Sci., 44, 748–760, 1987. 4348, 4351
Zink, F. and Vincent, R.: Wavelet analysis of stratospheric gravity wave packets over Macquarie Island, J. Geophys. Res., 106, 10 275–10 288, 2001. 4344, 4345

Table 1. Parameters of the VHF radar OSWIN at Kühlungsborn and the UHF Wind profiler at Lindenberg.

	OSWIN VHF Radar	UHF Wind Profiler
Geographical location	54.1° N, 11.8° E	52.2° N, 14.1° E
Operating frequency	53.5 MHz	482 MHz
Peak power/duty cycle	90 kW/5 %	16 kW/ 10 %
Transmitting antenna	144 Yagi array	Phased array (CoCo)
Antenna aperture (area)	1900 m^2	140 m^2
Half-power beam width	6°	3°
Pulse length	4 µs	3.3 µs
N of transmitter/receiver	6	1
Code	Single pulse	8-bit-Complementary code
Coherent integration	128	30
Vertical resolution	300 m	250 m
Altitude range	1–18 km	2.7–16.0 km
Time resolution	~1 min	~33 sec
Methods	DBS, (SA)	DBS

ACPD
4, 4339–4381, 2004

Table 2. Stokes parameters derived from radar measurements at 17 December 1999 for 5 h starting from 00:00 UT (Kühlungsborn) and 10:00 UT (Lindenberg). The data have been band pass filtered with cut-off frequencies corresponding to periods of 8–18 h in time and vertical wavelengths of 2–4.5 km, respectively.

Stokes parameters	Kühlungsborn	Lindenberg
Degree of polarization, d_{m_1,m_2}	0.88	0.79
Major axis orientation, Θ_{m_1,m_2}	50.5°	58.6°
Phase difference, δ_{m_1,m_2}	67.5°	63.4°
Ellipse axial ratio, R_{m_1,m_2}	0.66	0.58

ACPD
4, 4339–4381, 2004

Table 3. Stokes parameters derived from radar measurements at 17 December 1999 for 5 h starting from 00:00 UT (Kühlungsborn) and 07:00 UT (Lindenberg). The data have been band pass filtered with cut-off frequencies corresponding to periods of 2–8 h in time and vertical wavelengths of 2–4.5 km, respectively.

Stokes parameters	Kühlungsborn	Lindenberg
Degree of polarization, d_{m_1,m_2}	0.55	0.62
Major axis orientation, Θ_{m_1,m_2}	77.8°	88.1°
Phase difference, δ_{m_1,m_2}	79.9°	93.9°
Ellipse axial ratio, R_{m_1,m_2}	0.66	0.40

ACPD
4, 4339–4381, 2004

Table 4. Horizontal wavelengths and ground-based phase speeds as derived from the cross-spectral analysis in dependence on the wave direction and the vertical height shift for an observed period $2\pi/\omega_{ob}$ of −11.4 h and a distance $|S|$ between both radars of 265 km.

Case	Time delay τ, h	Major axis orientation Θ,°	Angle between $\boldsymbol{k}$ and $\boldsymbol{S}$ α,°(Fig. 10)	Vertical shift Δz, km	Horizontal wavelength $2\pi/k$, km	Observed horizontal phase speed υ_{ph}^{ob}, m/s
(A)	10.1	−6	48	0	−200	4.9
				−1.0	−304	7.4
				−2.0	−634	15.4
(B)	10.1	0	54	0	−176	4.3
				−1.0	−267	6.5
				−2.0	−557	13.6
(C)	−1.3	54	108	0	−714	17.4
				−0.5	−307	7.5
				−1.0	−195	4.8

ACPD
4, 4339–4381, 2004

Table 5. Gravity waves parameters at about 9 km derived from the the results of the Stokes-parameter analysis as shown in Table 2 for the radar measurements at Kühlungsbon and Lindenberg, using band pass filtered data with cut-off frequencies corresponding to periods of 8–18 h in time.

IGW parameters	Kühlungsborn	Lindenberg
Mean horizontal wind, $\overline{U}$, m/s (in the wave propagation direction)	17	18
Wind shear component, $\partial\overline{V}/\partial z$, s^{-1}	$2.8 \cdot 10^{-3}$	$-0.5 \cdot 10^{-3}$
Observed period, $2\pi/\omega_{ob}$, h	−11.4	−11.4
Intrinsic period, $2\pi/\omega_{in}$, h	7.7	8.3
Horizontal wavelength, $2\pi/k$, km	−281	−313
Vertical wavelength, $2\pi/m$, km	3.3	3.6
Horizontal phase velocity, υ_{ph}, m/s	−10.1	−10.3
Vertical phase velocity, υ_{pz}, m/s	0.11	0.12
Horizontal group velocity, c_{gh}, m/s	−6.6	−7.3
Vertical group velocity, c_{gz}, m/s	−0.08	−0.08

ACPD
4, 4339–4381, 2004

Table 6. Gravity waves parameters at about 6 km derived from the the results of the Stokes-parameter analysis as shown in Table 3 for the radar measurements at Kühlungsbon and Lindenberg, using band pass filtered data with cut-off frequencies corresponding to periods of 2–8 h in time.

IGW parameters	Kühlungsborn	Lindenberg
Mean horizontal wind, $\overline{U}$, m/s (in the wave propagation direction)	2.9	−1.3
Wind shear component, $\partial\overline{V}/\partial z$, s^{-1}	$-1.7 \cdot 10^{-3}$	$1.4 \cdot 10^{-5}$
Observed period, $2\pi/\omega_{ob}$, h	6.4	6.4
Intrinsic period, $2\pi/\omega_{in}$, h	8.3	6.0
Horizontal wavelength, $2\pi/k$, km	225	158
Vertical wavelength, $2\pi/m$, km	−3.2	−3.2
Horizontal phase velocity, υ_{ph}, m/s	7.5	7.3
Vertical phase velocity, υ_{pz}, m/s	−0.1	−0.15
Horizontal group velocity, c_{gh}, m/s	5.6	6.2
Vertical group velocity, c_{gz}, m/s	0.08	0.12

ACPD
4, 4339–4381, 2004

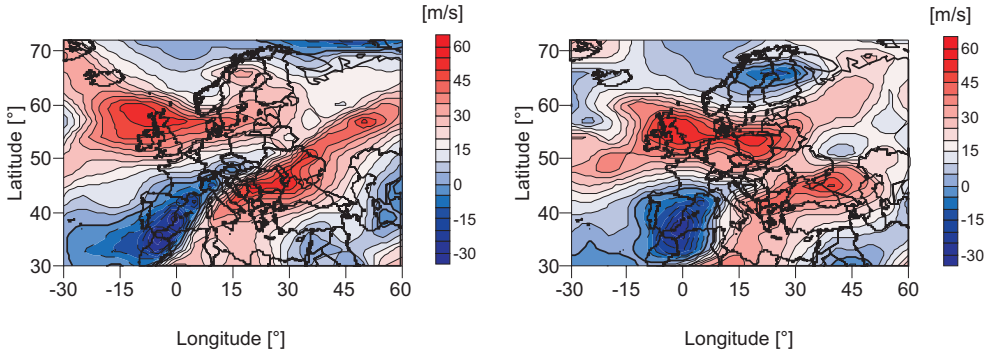

Fig. 1. Mean zonal wind derived from ECMWF analyses for the 300 hPa level at 17 December 1999, 12:00 UT (left) and 18 December 1999, 12:00 UT (right).

ACPD

4, 4339–4381, 2004

Investigation of inertia-gravity waves with collocated radars

A. Serafimovich et al.

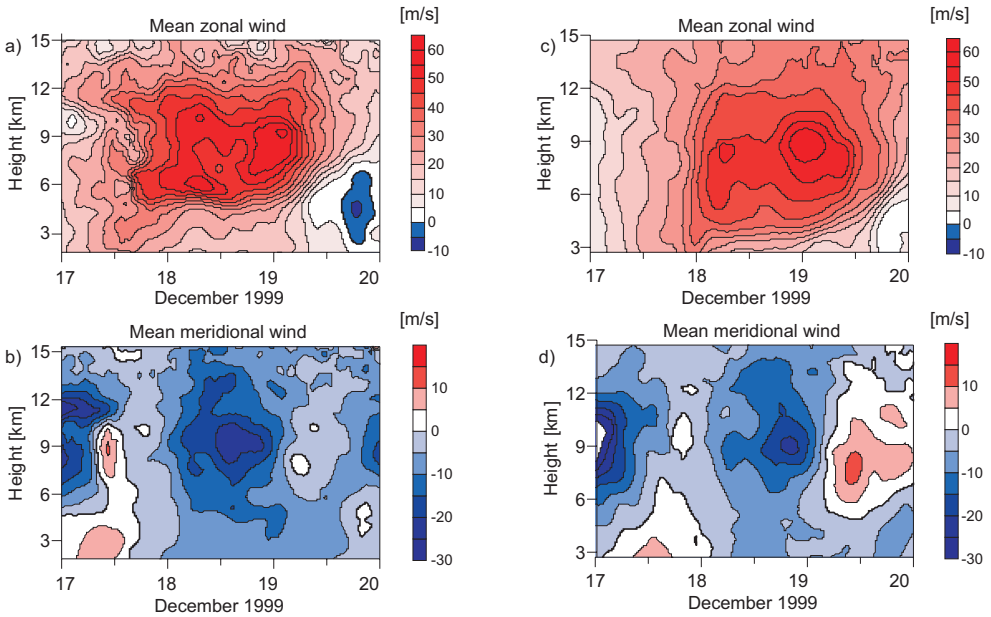

Fig. 2. Mean zonal and meridional winds measured at Kühlungsborn (**a, b**) and Lindenberg (**c, d**) from 17–19 December 1999. The data are smoothed using a low-pass filter with cut off frequencies corresponding to 4 h in time and 600 m in altitude.

ACPD
4, 4339–4381, 2004

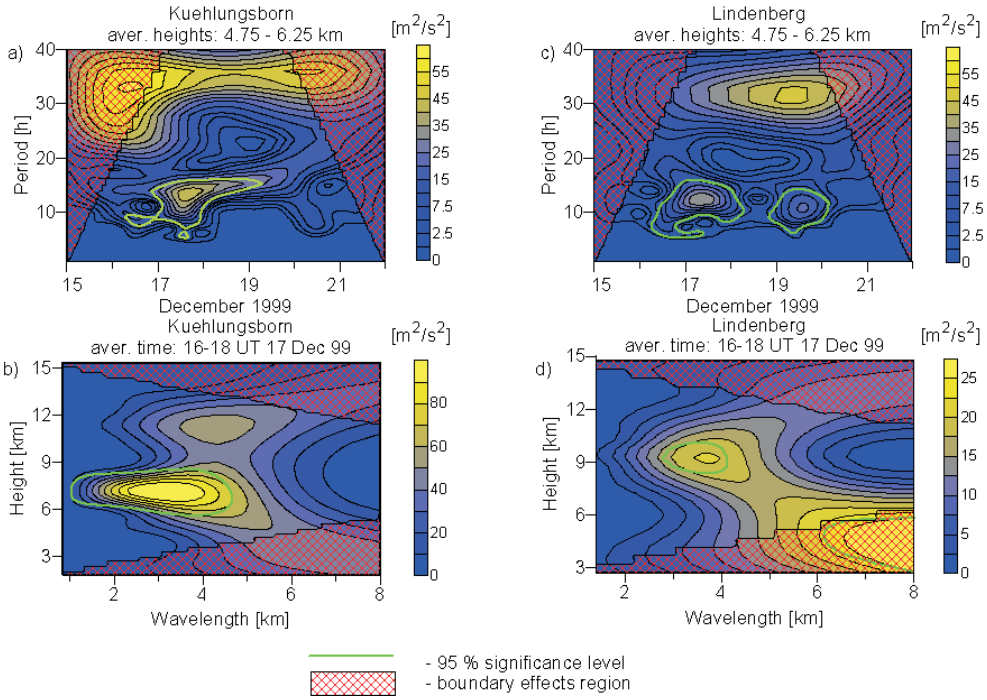

Fig. 3. Averaged sum of wavelet power spectra of the zonal and meridional winds measured at Kühlungsborn (**a, b**) and Lindenberg (**c, d**), in the upper panel (a, c) as wavelet transforms of the time series averaged over the altitude range from 4.75 to 6.25 km, in the lower panel (b, d) as wavelet transforms of the vertical wind profiles, respectively.

ACPD
4, 4339–4381, 2004

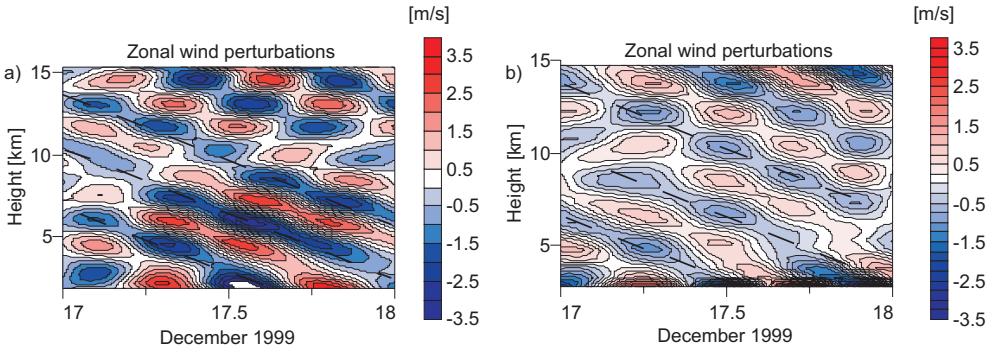

Fig. 4. Zonal wind perturbations at Kühlungsborn **(a)** and Lindenberg **(b)** for 17 December 1999 after band pass filtering with bandwidths of 8–18 h in time and 2–4.5 km in height.

ACPD

4, 4339–4381, 2004

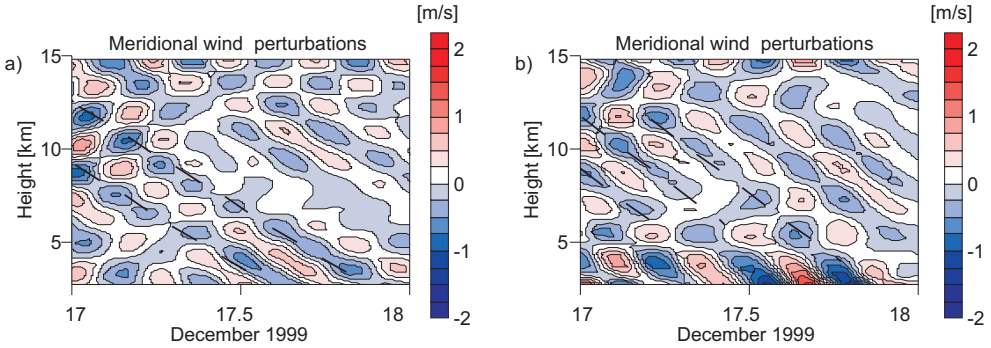

Fig. 5. Meridional wind perturbations at Kühlungsborn **(a)** and Lindenberg **(b)** for 17 December 1999 after band pass filtering with bandwidths of 2–8 h in time and 2–4.5 km in height.

ACPD
4, 4339–4381, 2004

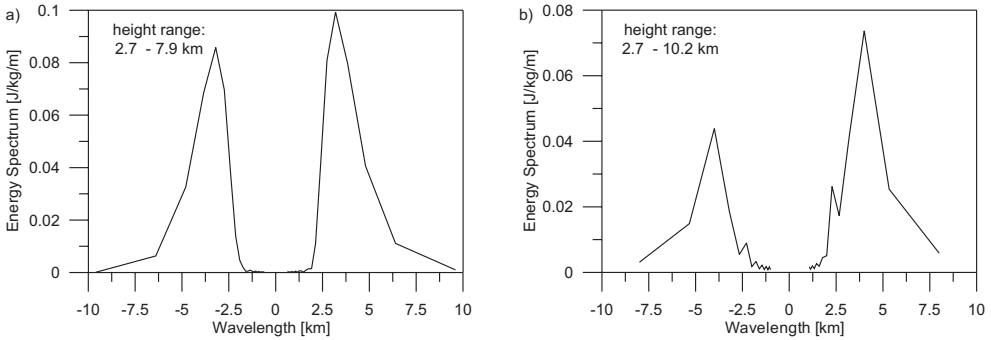

Fig. 6. Results of the rotary spectra averaged for 5 h at 17 December 1999 starting from 10:00 UT for Kühlungsborn **(a)** and 19:00 UT for Lindenberg **(b)** after band pass filtering with bandwidths of 8–18 h in time and 2–4.5 km in height.

ACPD
4, 4339–4381, 2004

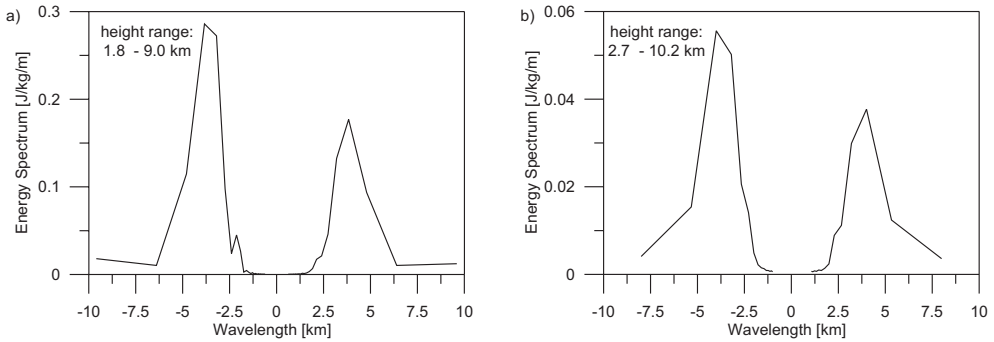

Fig. 7. Results of the rotary spectra averaged for 5 h at 17 December 1999 starting from 07:00 UT for Kühlungsborn **(a)** and 09:30 UT for Lindenberg **(b)** after band pass filtering with bandwidths of 2–8 h in time and 2–4.5 km in height.

ACPD
4, 4339–4381, 2004

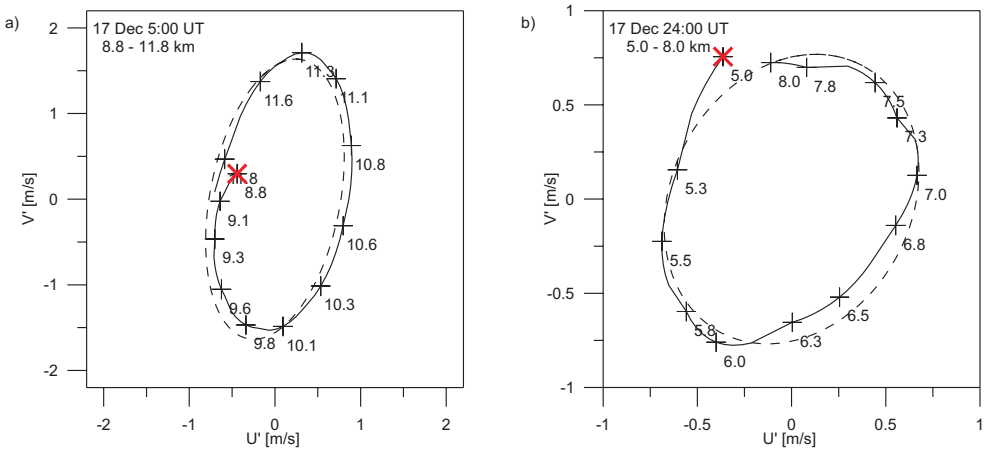

Fig. 8. Results of hodograph analyses for the wind perturbations after band pass filtering with bandwidths of 8–18 h in time and 2–4.5 km in height (solid line – measured profiles, dashed line – fitted ellipse, **X** – starting point of the hodograph), applied to radar measurements at Kühlungsborn **(a)** and Lindenberg **(b)**.

ACPD
4, 4339–4381, 2004

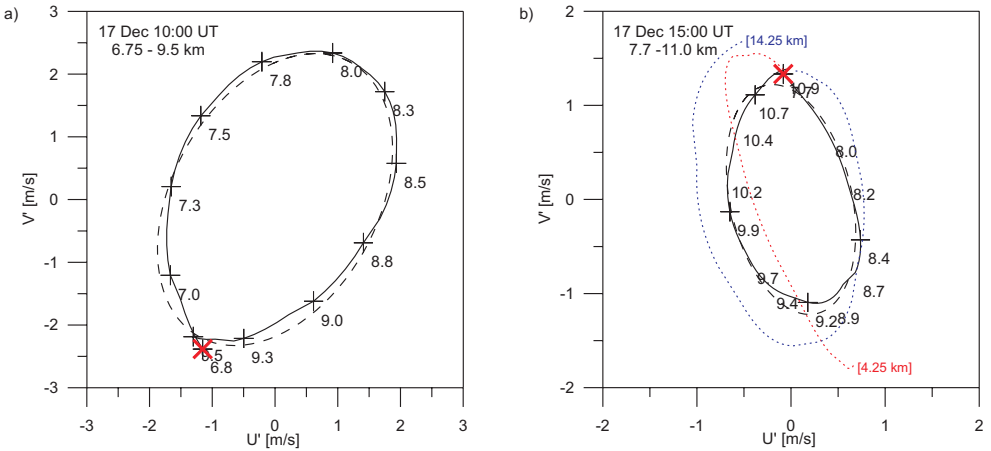

Fig. 9. Results of the hodograph analysis applied on the wind perturbations after band pass filtering with bandwidths of 2–8 h in time and 2–4.5 km in height (solid line – measured profiles, dashed line – fitted ellipse, **X** – starting point of the hodograph), applied to radar measurements at Kühlungsborn **(a)** and Lindenberg **(b)**. In (b), the hodograph has been extendend from 4.25–7.7 km (red dashed line) and from 11.0–14.25 km (blue dashed line).

ACPD
4, 4339–4381, 2004

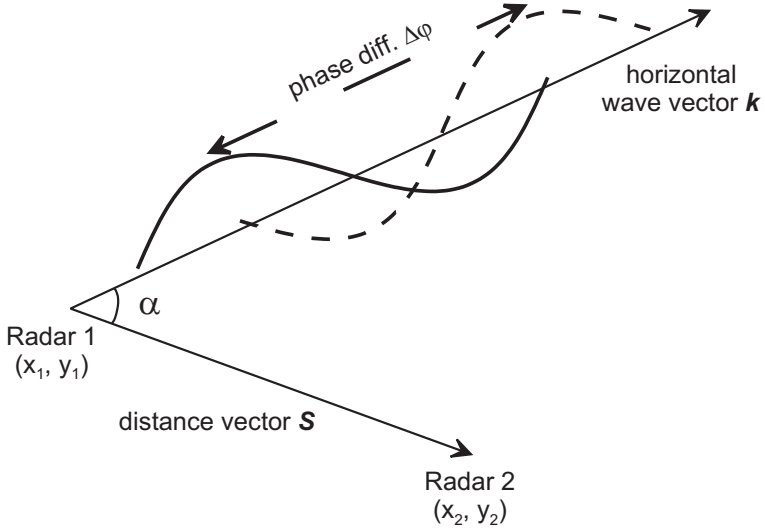

Fig. 10. Block-scheme of IGW propagation.

ACPD
4, 4339–4381, 2004

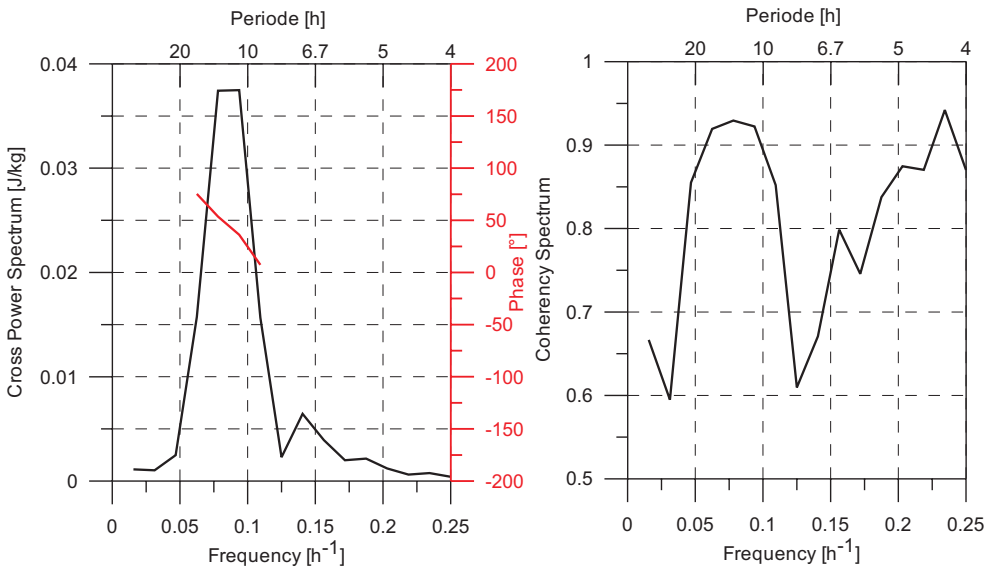

Fig. 11. Cross-power spectrum between radar measurements at Kühlungsborn and Lindenberg for the time from 17 December 1999, 00:00 UT to 18 December 1999, 00:00 UT, averaged over the height range from 5.25 km to 7.75 km. Left part: Amplitude (black) and phase difference (red). Right part: Coherency spectra.

ACPD
4, 4339–4381, 2004

Investigation of inertia-gravity waves with collocated radars

A. Serafimovich et al.